

# A Land–Atmosphere Interaction Theory for the Tropical Deforestation Problem

NING ZENG AND J. DAVID NEELIN

*Department of Atmospheric Sciences and Institute of Geophysics and Planetary Physics, University of California, Los Angeles, Los Angeles, California*

(Manuscript received 15 January 1998, in final form 15 April 1998)

## ABSTRACT

A theoretical framework is developed in understanding the mechanisms and processes determining the response of the land–atmosphere system to tropical deforestation. The analytical approach is made possible by simplifications in the vertical from the quasi-equilibrium moist convective closure, and in the horizontal from the dynamical temperature homogenization process. The theory emphasizes the energy and water balance. It highlights the interaction among processes of moist convection, cloud, radiation, and surface hydrology while each individual process is simplified. The zero surface energy flux condition, due to the small heat capacity of land, makes land–atmosphere interaction distinctly different from ocean–atmosphere interaction. This imposes a constraint on the sensitivity to the details of surface energy partitioning. Consequently, land surface temperature is largely a response to the energy and water balance, rather than a forcing as in the case of sea surface temperature.

Results from a wet-season surface albedo change case compare well with a recent RCM2/BATS simulation, with the theory depicting the mechanisms and the roles of the intertwining processes. The precipitation has a significant decrease, initiated by ground radiative forcing as increased surface albedo reflects more solar radiation into space. A positive feedback by moisture convergence is essential for this tendency, with another positive feedback from reduced evaporation providing further enhancement. These are opposed by a negative feedback due to the reduced magnitude of negative cloud radiative forcing as cloud cover decreases. This sheds light on the higher sensitivity in some GCM studies with prescribed clouds. The cloud radiative forcing also has a negative feedback on the initial cooling tendency in ground temperature. Together with reduced evaporation, this leads to little change in the ground temperature. Sensitivities of precipitation and ground temperature changes to individual processes are found to depend on the reference state parameter values, implying a sensitivity of anomaly response to simulated climatology for GCMs. The analysis here also serves as an example of the tight coupling between convection, large-scale atmospheric dynamics, and land processes in the tropical land–atmosphere system.

## 1. Introduction

The main rainfall centers in the Tropics are located over the three main tropical landmasses: central Africa, the Maritime Continent, and the Amazon. A mean annual rainfall of over 2000 mm sustains the world's most diverse ecosystem in the tropical rain forest, which in turn exchanges energy, water, and momentum with the atmosphere. Although climate models are capable of simulating a reasonably realistic rain forest climate given a prescribed surface condition, we do not understand well the sensitivity of the coupled climate–ecosystem nor how it is established in the first place.

Recent GCM studies have suggested a possible change in regional climate under a scenario of basinwide Amazon deforestation [see Hahmann and Dickinson

(1997), hereafter HD, Table 1 for a summary and references therein]. Most experiments have found a significant reduction in precipitation and evaporation. Most also find a reduction in moisture convergence but there is not general agreement even on the sign of this change (Lean et al. 1996). More questions arise as to the roles of different land surface properties such as albedo and roughness. Further complication comes when considering model response to the current level of deforestation as mesoscale effects become important (Eltahir and Bras 1994; Walker et al. 1995).

Although much progress has been made in understanding the individual model behavior (e.g., Polcher 1995; Zhang et al. 1996), the complexity of GCMs hinders our ability to fully depict the cause–response relationship and to understand the disparities among the GCM experiments. Much attention has been paid to detailed land surface representation, leaving the host GCMs to take care of the atmospheric modeling. The key processes determining the deforestation response both in the atmosphere and over land are not clearly identified nor well understood. For instance, tropical

---

*Corresponding author address:* Dr. Ning Zeng, Department of Atmospheric Sciences, University of California, Los Angeles, CA 90095-1565.  
E-mail: zeng@atmos.ucla.edu.

rainfall is mainly convective and the associated clouds play an important role in the energy budget. Current GCMs use a wide range of moist convective and cloud-radiation parameterization schemes (Gates et al. 1995). How much of the difference among the deforestation experiments can be attributed to this is not clear. Manzi and Planton (1996) studied the Amazon deforestation response using two different moist convective parameterizations in the same GCM. And the results were found to be significantly different. Polcher (1995) further showed that different convective schemes produce different frequencies of occurrence of deep convective events. Land surface processes are equally complicated. To determine which are the important ones and how they interact with boundary layer and moist convection remains a challenge. It is difficult to cross-examine simulations with different land surface schemes and host GCMs, but theoretical understanding can help delineate the key processes and mechanisms.

Charney's (1975) theory of the albedo influence on Sahel rainfall stimulated the study of land-atmosphere interaction. Eltahir and Bras (1993) developed a simple model to interpret some early Amazon deforestation GCM results, highlighting the competing feedback effects of a warmer surface and less precipitation, both of which can result from a reduction in evaporation. In an intermediate-level model and subsequent analysis, Zeng et al. (1996) and Zeng (1998) showed that the deforestation response is largely determined by a three-way balance among large-scale adiabatic cooling, convective heating, and radiation.

Building on experience from GCM experiments and these earlier analyses, the present work attempts to provide a comprehensive picture of the tropical rain forest climate system. The approach is to simplify the individual processes but to focus on the interactions among them. Thereby the relative importance of these processes can be delineated, and the range of sensitivity to the strength of each individual process can then be explored. The analytical framework is made possible by the following:

- Moist convection imposes constraints on vertical temperature and humidity profiles and subsequent redistribution of energy occurs subject to this constraint (Arakawa and Schubert 1974; Betts and Miller 1986).
- The feedback from the remote large-scale response occurs via convergence terms, whereas details of the spatial pattern of temperature and moisture response are negligible, so one does not need to solve the full dynamical equations.
- Small perturbations on a climatologically deep convective region are considered so that the processes can be linearized.

In this context a perturbation means the "deforestation-minus-control" type of experiment as typically done in GCM sensitivity studies where the present climate system (control) is compared to a hypothetical climate sys-

tem with a different boundary condition (deforestation) that is in its own equilibrium climate. Thus a perturbation as defined here is the difference between the two systems. Linearization will not always be valid for such changes, but to the extent that it holds, it can give insight into processes. The analysis here holds best if both states have sufficient convection over the target region so the quasi-equilibrium assumption applies to both.

In this work we focus on the atmospheric component and surface energy balance. More details of surface hydrology and other aspects of deforestation will be addressed in follow-up work. In section 2 we introduce the ingredients of the theory. Then this is applied to a wet-season albedo change case in section 3. Some processes and mechanisms are analyzed in section 4. In section 5 we discuss caveats and the implications for GCM studies.

## 2. Theory

### a. Energy and water budget

We start with the thermodynamic equation and moisture equation:

$$C_p \left( \frac{\partial}{\partial t} + \mathbf{v} \cdot \nabla \right) T + \frac{\partial(C_p T + gz)}{\partial p} \omega = Q_c + Q_r + \frac{\partial F_T}{\partial p} \quad (2.1)$$

and

$$L \left( \frac{\partial}{\partial t} + \mathbf{v} \cdot \nabla \right) q + L \frac{\partial q}{\partial p} \omega = Q_q + \frac{\partial F_q}{\partial p}, \quad (2.2)$$

where  $\mathbf{v} \cdot \nabla$  is horizontal advection and  $\omega$  is large-scale vertical velocity in pressure coordinates. Throughout this article, water fluxes including precipitation, evaporation, and moisture convergence are expressed in energy units (multiplying by latent heat  $L$ ). Here  $Q_c$  and  $Q_r$  are convective and radiative heating, respectively, and  $Q_q$  is moisture source due to condensation. Here  $F_T$  and  $F_q$  are vertical diffusive fluxes of sensible heat and moisture, with boundary values being surface sensible heat flux and evaporation. At the seasonal timescale and basin spatial scale of concern here, the flow is quasi-steady so the time derivatives can be neglected. The spatial distribution of tropical temperature and humidity are much smoother than the wind field, so that the horizontal advection can also be neglected to a first approximation (Zeng 1998).

Under the quasi-equilibrium assumption (Arakawa and Schubert 1974) convection tends to establish statistical equilibrium between large-scale dynamics and local moist convection and therefore constrains the vertical temperature and moisture profiles. Betts and Miller (1986) found the profiles are very close to a virtual moist adiabat at deep convective regions both over ocean and land. In a deep convective region, this constraint ties

the boundary layer temperature together with the free atmosphere temperature, but they are not coupled to ground temperature although processes such as sensible heat tend to pull them together (see section 4b on the processes controlling ground temperature). Following Emanuel et al. (1994), Neelin and Yu (1994), Neelin and Zeng (1998, manuscript submitted to *J. Atmos. Sci.*) the constraint on temperature leads to a constraint on vertical profile of horizontal velocity and thus a constraint on the profile of vertical velocity through the continuity equation:

$$\omega(x, y, p) = \Omega(p)\nabla \cdot \mathbf{v}_1(x, y),$$

and it has been split into a vertical dependence  $\Omega(p)$  given by the hydrostatic equation and constraint on temperature profile, and a horizontal dependence  $\mathbf{v}_1(\mathbf{x}, \mathbf{y})$ . The vertical profile  $\Omega(p)$  is solely determined by the quasi-equilibrium temperature profile. As one goes away from deep convective region, this constraint holds less well. This point is of relevance when the Amazon is in its dry season so more care would be required in application of the current theory.

Now vertically integrating Eqs. (2.1) and (2.2) using this constraint,

$$M_s \nabla \cdot \mathbf{v}_1 = \hat{Q}_C + \hat{Q}_R + H, \quad (2.3)$$

$$-M_q \nabla \cdot \mathbf{v}_1 = \hat{Q}_q + E, \quad (2.4)$$

where  $E$  is evaporation,  $H$  is sensible heat flux, and a hat or angles define the vertical integral:  $\langle \cdot \rangle \equiv \langle (\cdot) \rangle \equiv (1/g) \int_{p_t}^{p_0} (\cdot) dp$  with  $p_0$  and  $p_t$  pressure at the surface and the tropopause, such that the quantities are in units of energy flux. The vertically integrated dry static stability is

$$M_s = \left\langle \frac{\partial(C_p T + gz)}{\partial p} \Omega \right\rangle$$

and the moisture stratification

$$M_q = \left\langle -\frac{\partial(Lq)}{\partial p} \Omega \right\rangle.$$

Equation (2.4) is the vertically integrated water budget equation:

$$-C = -P + E, \quad (2.5)$$

where  $C$  is vertically integrated moisture convergence and  $P$  is precipitation, with  $C = M_q \nabla \cdot \mathbf{v}_1$  and  $P = -\hat{Q}_q$ . Note that (2.5) returns the advection of moisture so it is a more precise relation than (2.4). It is very useful to consider the sum of (2.3) and (2.4), the moist static energy equation:

$$mC = \hat{Q}_R + E + H, \quad (2.6)$$

where  $m \equiv M/M_q$  is the ratio between the gross moist stability  $M \equiv M_s - M_q$  and the moisture stratification. In deriving (2.6) the enthalpy conservation constraint  $\hat{Q}_C + \hat{Q}_q = 0$  has been used.

Surface-atmosphere energy and water budget

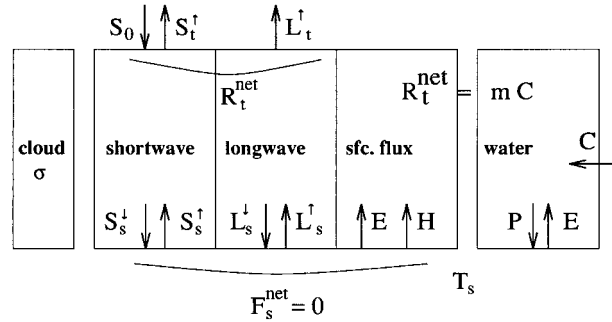


FIG. 1. Schematic diagram for the energy and water budget at the top of the atmosphere and at the surface, showing notation. The rightmost box shows the atmospheric water budget; the three center boxes show the energy fluxes into and out of the atmosphere; the leftmost box is used to display cloud fraction contribution in subsequent figures.

At the top of the atmosphere and the surface, the net downward energy fluxes are

$$R_t^{\text{net}} = S_0 - S_t^{\uparrow} - L_t^{\uparrow}$$

$$F_s^{\text{net}} = S_s^{\downarrow} - S_s^{\uparrow} + L_s^{\downarrow} - L_s^{\uparrow} - E - H,$$

where  $S$  and  $L$  denote shortwave and longwave radiative fluxes, respectively, with arrows indicating upward or downward direction. Figure 1 summarizes notation; quantities (including anomalies) are defined to have positive sign in the direction of the arrows. Subscripts  $_s$  and  $_t$  denote surface and top of the atmosphere, respectively. Then (2.6) can be rewritten as

$$mC = R_t^{\text{net}} - F_s^{\text{net}}, \quad (2.7)$$

where we have used the identity

$$\hat{Q}_R = S_0 - S_t^{\uparrow} - S_s^{\downarrow} + S_s^{\uparrow} - L_s^{\downarrow} + L_s^{\uparrow} - L_t^{\uparrow}.$$

Equation (2.7) simply states that in a deep convective region, the total energy and water flux absorbed in the atmospheric column drives a moisture convergence, and the effectiveness of this forcing depends on the relative moist stability factor  $m$ . The more/less stable (larger/smaller  $m$ ) the less/more moisture convergence a certain forcing can drive. Thus  $m$  is a key parameter here. To further understand the role of moist processes, we define  $\tilde{q} \equiv M_q/M_s$ . Typically  $M_q$  is only slightly smaller than  $M_s$  (Yu et al. 1998) so that  $\tilde{q} \approx 1$  or  $1 - \tilde{q} \ll 1$ . If the gross moist stability  $M$  is scaled by the dry stability  $M_s$ :

$$\frac{M}{M_s} = m\tilde{q} = 1 - \tilde{q}.$$

This is similar to the moisture convergence feedback of Webster (1981), Zebiak (1986), Zeng (1998), and others, except here the moist process is “built in” based on the quasi-equilibrium assumption. It is also similar to  $1 - \epsilon$  of Emanuel et al. (1994), where  $\epsilon$  is interpreted as a

precipitation efficiency associated with downdraft re-evaporation. Though different in interpretation, the formulations are mathematically similar. In any case,  $m$  is a highly lumped parameter absorbing all the effects involved in subgrid-scale moist convective processes, including mesoscale effects. Yu et al. (1998) analyzed this gross moist stability based on observational data, and found a reasonably robust estimate for the tropical deep convective regions.

Over land, because of land's low heat capacity and lack of transport (as opposed to the ocean), the surface flux is nearly zero on timescales longer than the diurnal or synoptic scale:

$$F_s^{\text{net}} = 0. \quad (2.8)$$

This condition is explicitly used in some GCMs such as the National Center for Atmospheric Research Community Climate Model, version 1 (NCAR CCM1; Williamson et al. 1987). Thus over land

$$mC = R_t^{\text{net}}. \quad (2.9)$$

This is at the core of the theory. It makes the crucial link between the energy budget and the water budget (Fig. 1). This simple relation leads to some interesting insights. For instance, the top of the atmosphere net radiation is a well-measured quantity given by, say, the Earth Radiation Budget Experiment (ERBE; Harrison et al. 1993). We can use this information to derive the moisture convergence for tropical convective land region, assuming the stability  $m$  is known (which depends on convective characteristics). ERBE data can be used to constrain the parameters in the theory through this relation and the application for diagnosing GCM results will be discussed later.

To further understand the implication of this relationship, consider an example of the tropical climatology where the continent regions, namely, the Amazon, central Africa, and the Maritime Continent tend to be the major convective centers. The question arises as to how land compares with ocean in competing for moisture convergence. The net surface flux  $F_s^{\text{net}}$  in (2.7) is zero over land but is generally positive over tropical ocean where heat is absorbed and transported away by ocean currents or mixing. Thus in a zonally averaged sense the tropical land is in a favored position for getting moisture convergence. However, the divergence of ocean heat transport differs greatly from region to region, so some regions, such as the western Pacific warm pool, are not at all disfavored, whereas others, such as the eastern Pacific are considerably disfavored. The warm pool surface flux is only slightly positive into the ocean [ $F_s^{\text{net}}$  slightly greater than zero in (2.7); Oberhuber 1988] so the convection there is comparable to that over the adjacent Maritime Continent (assuming the convective characteristics, and therefore the stability factor  $m$ , are not significantly different).

This exposes a common problem in tropical simple models where the land is treated like an ocean with

prescribed (usually observed) surface temperature. In this case total surface flux  $F_s^{\text{net}}$  varies with atmospheric condition and can be far from zero. The "land" then supplies or sucks energy out of nowhere, leading to potentially higher sensitivity than for a land surface constrained by the flux zero condition (2.8). An example of this is discussed in section 4a.

### b. Surface fluxes

The determination of  $E$  can require a full surface hydrology scheme and it involves complicated interaction between the energy and the water cycles. Our analysis shows that given the abundant available radiation in the Tropics, the water budget is the dominating factor on the seasonal timescale of concern here. Thus how precipitation is partitioned into runoff and evaporation becomes the key. The interplay between evaporation and runoff is complex and handled quite differently in current land surface parameterization schemes (Koster and Milly 1997). In this paper we work with a general form:

$$E' = eP', \quad (2.10)$$

where a prime denotes perturbation. Appendix A gives a derivation of this based on a single soil-layer model representing the root zone. The perturbation evaporation efficiency factor  $e$  depends on interception and evapotranspiration, and indirectly on runoff. An estimate of  $e$  can be made by specifying the parameterizations of these processes, but the justification of the use of particular functional dependences will quickly become quite involved. In the present work we will treat the evaporation efficiency factor  $e$  as a tunable parameter such that the predicted evaporation change is the same as that predicted by a GCM in the case of quantitative comparison.

Sensible heat is parameterized by a bulk transfer formula

$$H = \zeta(T_s - T), \quad (2.11)$$

where  $\zeta = C_p \rho C_D V_s$  absorbs air density  $\rho$ , drag coefficient  $C_D$ , and surface wind speed  $V_s$ .

### c. Cloud and radiation

The change in cloud cover is found to play a prominent role in the surface energy budget in Amazon deforestation GCM studies (Dickinson and Kennedy 1992; Zhang et al. 1996). We can only predict deep convective cloud that has a simple relationship with convective precipitation (e.g., Slingo and Slingo 1991; Chou 1997). Fortunately, other radiatively important types of clouds over tropical land are mostly associated with deep convective clouds, so a simple approach can capture the first-order effects. In this approach, high and middle clouds are lumped together as one cloud type and the cloud cover  $\sigma$  is determined by deep convective pre-

precipitation, which accounts for most of the tropical rainfall:

$$\sigma = \sigma_p P. \quad (2.12)$$

The coefficient  $\sigma_p$  is deduced from a linear regression of observed precipitation and the International Satellite Cloud Climatology Project (ISCCP; Rossow and Schiffer 1991) cloud cover (Chou 1997) for tropical climatology. The low cloud is assumed not to change so much as to be radiatively important for the deforestation problem. These simple assumptions, of course, can be refined.

We now have a closed system of Eqs. (2.8)–(2.12). We also need to express the radiation in terms of temperature, humidity, and cloud cover, etc. For shortwave radiation, we have derived a simple formula (see appendix B for details), assuming a single cloud–atmosphere layer with reflectivity  $\alpha$  and absorptivity  $a$ , and a ground with albedo  $A$ . If small perturbations are introduced in the cloud reflectivity and ground albedo, one obtains for the linearized shortwave fluxes

$$S'_t/S_0 = -\theta_{tA}A' - \theta_{t\alpha}\alpha',$$

$$S'_s/S_0 = -\theta_{sA}A' - \theta_{s\alpha}\alpha',$$

where  $S_t$  and  $S_s$  are net downward solar at top and surface, respectively. The linearization coefficient  $\theta$  measures the fraction of solar radiation associated with a given cloud or surface albedo change, taking into account other loss factors.

Cloud albedo  $\alpha$  is assumed to be linearly proportional to the cloud cover (appendix B):

$$\alpha = \alpha_\sigma \sigma. \quad (2.13)$$

A solar zenith angle dependence is approximated and absorbed in  $\alpha_\sigma$ .

Chou and Neelin (1996) found longwave radiation can be well approximated by a linear scheme, perturbed about a tropical reference profile. Linearizing longwave radiative fluxes

$$L_s^{\downarrow'} = \epsilon_{st}T' + \epsilon_{sq}q' + \epsilon_{s\sigma}\sigma',$$

$$L_t^{\uparrow'} = \epsilon_{tT}T' + \epsilon_{tq}q' + \epsilon_{t\sigma}\sigma',$$

$$L_s^{\uparrow'} = \epsilon_s T'_s,$$

where prime denotes a deviation from the corresponding mean, and  $\epsilon$  is the slope of the nonlinear relation at its mean. Here  $T'$ ,  $q'$ , and  $\sigma'$  are the perturbation amplitudes of the reference profiles. Because of the nonlocality of radiative contribution from different heights, the  $\epsilon$ 's are convolutions of Green's function and the assumed vertical profiles. The contribution to  $L_t^{\uparrow'}$  from surface temperature  $T'_s$  is quite small and has been neglected.

The determination of  $T'$  and  $q'$  depends on large-scale dynamics as well as local perturbation, and is therefore difficult to quantify in a simple model. However, for purposes here,  $T'$  is negligible. The basic rea-

son is that any localized temperature perturbation is spread out by a Helmholtz-like operator so that the temperature is homogenized within the radius of deformation (e.g., Held and Hou 1980). Zeng (1998) estimates that the actual temperature relative to a radiative–convective equilibrium temperature  $T^*$  is about 0.04 for the Amazon region. The contributions to IR from  $T'$  and  $q'$  (assuming constant relative humidity) are negligible compared to cloud effects. Thus, to first-order approximation, the large-scale dynamics comes in only through the moisture convergence term representing large-scale adiabatic cooling and drying effects, which can be solved without considering remote dynamics. In this sense the large-scale response is merely a “response” to local thermodynamic forcing. Once the vertical profiles of mean temperature and moisture are specified the model can be solved locally within the convergence zone. One can then diagnose the anomaly flow fields and horizontal temperature structure associated with the local disturbance. But the horizontal structure is not needed for the purposes here.

### 3. Climate sensitivity to surface albedo change in a deep convective region

We now consider a case where a small change in surface albedo is made. Perturbations (primed) denote the difference between two equilibrium climates of different surface albedo. The Eqs. (2.5), (2.8)–(2.13) are

$$mC' = -S_0(\theta_{tA}A' + \theta_{t\alpha}\alpha') - \epsilon_{t\sigma}\sigma', \quad (3.1)$$

$$0 = -S_0(\theta_{sA}A' + \theta_{s\alpha}\alpha') - \epsilon_s T'_s + \epsilon_{s\sigma}\sigma' - E' - H', \quad (3.2)$$

$$P' = E' + C', \quad (3.3)$$

$$E' = eP', \quad (3.4)$$

$$H' = \zeta T'_s, \quad (3.5)$$

$$\sigma' = \sigma_p P', \quad (3.6)$$

$$\alpha' = \alpha_\sigma \sigma', \quad (3.7)$$

where we have used the linearized solar and longwave radiation and dropped the  $T'$  and  $q'$  terms. Equations (3.1)–(3.7) form a closed system for variables  $P'$ ,  $E'$ ,  $C'$ ,  $H'$ ,  $\sigma'$ ,  $\alpha'$ , and  $T'_s$ .

We solve for  $P'$  from Eqs. (3.1), (3.3), (3.4), (3.6), and (3.7), which do not involve the surface fluxes other than evaporation:

$$P' = \frac{-S_0\theta_{tA}}{m(1-e) + c_t}A', \quad (3.8)$$

$E'$ ,  $C'$ ,  $\sigma'$ ,  $\alpha'$  are most easily expressed in terms of  $P'$ :

$$E' = eP',$$

$$C' = (1-e)P',$$

$$\sigma' = \sigma_p P',$$

$$\alpha' = \alpha_\sigma \sigma_p P'.$$

TABLE 1. Parameter values used in the theory. Estimated from various sources; see text for detail. Here LW is longwave.

Parameter	Symbol	Value
Relative moist stability	$m$	0.33
Cloud albedo–cover ratio	$\alpha_\sigma$	0.36
Cloud cover–precipitation ratio	$\sigma_p$	0.0029 100% W <sup>-1</sup> m <sup>2</sup>
Cloud upward LW at top	$\epsilon_{\sigma\sigma}$	–70 W m <sup>-2</sup> /100%
Cloud downward LW at surface	$\epsilon_{s\sigma}$	18 W m <sup>-2</sup> /100%
Ground temperature upward LW	$\epsilon_s$	6 W m <sup>-2</sup> K <sup>-1</sup>
Sensible heat factor	$\zeta$	100 W m <sup>-2</sup> K <sup>-1</sup>
$E$ – $P$ ratio	$e$	0.31
Incoming solar radiation	$S_0$	443 W m <sup>-2</sup>
Reference atmosphere absorptivity	$a$	0.28
Reference cloud–atmosphere reflectivity	$\alpha$	0.32
Reference surface albedo	$A$	0.13

We define cloud radiative forcing factors at top  $c_t$  and at surface  $c_s$ ,

$$c_t = (\alpha_\sigma \theta_{t\alpha} S_0 + \epsilon_{\sigma\sigma}) \sigma_p, \quad (3.9)$$

$$c_s = (\alpha_\sigma \theta_{s\alpha} S_0 - \epsilon_{s\sigma}) \sigma_p, \quad (3.10)$$

such that the cloud radiative forcing (CRF) at top and surface can be written as

$$\text{CRF}'_t = -c_t P',$$

$$\text{CRF}'_s = -c_s P'.$$

Note that  $\epsilon_{\sigma\sigma}$  is negative so longwave and shortwave cloud radiative forcing tend to act against each other both at the top and the surface. Solving for  $T'_s$  using (3.2) and (3.5),

$$\begin{aligned} (\epsilon_s + \zeta) T'_s &= -S_0 \theta_{sA} A' - (e + c_s) P' \\ &= -S_0 A' \left\{ \theta_{sA} - \frac{e + c_s}{m(1 - e) + c_t} \theta_{tA} \right\}. \end{aligned} \quad (3.11)$$

There is a cancellation in the two terms on the rhs of (3.11) so that  $T'_s$  may be small. More importantly, because of the large surface drag caused by the high roughness of the rain forest (large  $\zeta$ ), a slight change in surface temperature is sufficient to compensate the energy adjustment through the change in sensible heat flux.

Besides the above seven variables, analytical expressions for other quantities can be derived. For instance, using (B3) and (3.8), the top of the atmosphere outgoing shortwave radiation is

$$S_t^{\uparrow} = S_0 \theta_{tA} A' \left\{ 1 - \frac{\alpha_\sigma \sigma_p S_0}{m(1 - e) + c_t} \right\}. \quad (3.12)$$

Given estimated parameter values one can calculate the changes of all the variables. This gives a full picture of the energy and water balance in the column and enables a direct comparison with GCM results such as those of HD. Table 1 lists the values of parameters used and Table 2 gives the values of some important derived parameters that characterize the roles of the processes.

TABLE 2. Derived parameters. Here SW is shortwave.

Parameter	Symbol	Value
Cloud albedo SW coefficient top; (B3)	$\theta_{t\alpha}$	1
Cloud albedo SW coefficient surface	$\theta_{s\alpha}$	0.72
Surface albedo SW coefficient surface	$\theta_{sA}$	0.49
Surface albedo SW coefficient top	$\theta_{tA}$	0.31
CRF factor at top; see (3.9)	$c_t$	0.26
CRF factor at surface; see (3.10)	$c_s$	0.28
Moisture + evap. feedback factor	$m(1 - e)$	0.23

The relative moist stability parameter  $m$  is calculated from the expressions in section 2 using the European Centre for Medium-Range Weather Forecasts monthly mean vertical profiles of temperature and humidity for a deep convective region similar to Yu et al. (1998). The mean cloud–atmosphere absorptivity and reflectivity are derived from ERBE radiation budget and ISCCP cloud cover. The cloud albedo and cloud cover relation is derived from Bishop and Rossow's (1991) fast scheme, with an approximate account of solar zenith angle dependence following Chou (1997). The linearized longwave coefficients for cloud cover and ground temperature perturbation are calculated using Chou and Neelin's (1996) scheme. The cloud cover dependence on precipitation comes from a linear regression of ISCCP cloud cover and observed precipitation. The sensible heat coefficient corresponds to an aerodynamic resistance of 10 s m<sup>-1</sup>, typical for a tropical rain forest (e.g., Shuttleworth 1988). Further details can be found in corresponding sections describing these processes. For now (see section 2b), the evaporation factor  $e$  is tuned to produce the same evaporation as HD. The ground albedo is increased by 0.07 as in HD for comparison.

The theoretical results for the wet-season albedo change case are shown in Fig 2. Also shown are the RCM2 Biosphere–Atmosphere Transfer Scheme (BATS; Dickinson et al. 1993) results of HD for the corresponding case [i.e., December–February (DJF) albedo change only; some analyses for this case are not published in HD; courtesy of A. Hahmann]. The agreement in the water budget is good, considering the simplicity of the theory. Because the evaporation is forced to be the same and only two variables are independent due to the water budget requirement, the theory is really predicting only one variable. The identical appearance (up to a truncation error) is perhaps only coincidence. It is of interest to note that more recent GCM studies appear to be predicting less change in the hydrological cycle compared to some early GCM simulations (e.g., HD; Lean et al. 1996) although this is complicated by the spatial inhomogeneity in the response. The energy fluxes are also reasonably close, especially in surface radiative fluxes.

The most noticeable difference is the outgoing solar radiation where HD has a 4 W m<sup>-2</sup> increase, whereas the theory predicts only 0.5 W m<sup>-2</sup>. Despite the non-

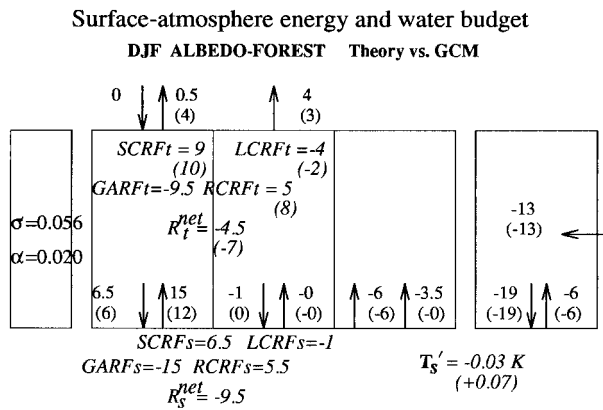


FIG. 2. Changes predicted by the theory, for the wet season and an albedo increase of 0.07. Numbers in the brackets are for the same case but from Hahmann and Dickinson (1997). See text and Fig. 1 for definition of the fluxes. SCRF is shortwave cloud radiative forcing; LCRF is longwave cloud radiative forcing; RCRF is net cloud radiative forcing; GARF is ground albedo radiative forcing;  $R_t^{net}$  is net radiation; and subscripts <sub>s</sub> and <sub>t</sub> denote surface and top, respectively. The fluxes are all in  $W m^{-2}$ ; to convert to  $mm day^{-1}$  for water fluxes, divide by 28.

trivial difference in the top of the atmosphere net radiation, the theory and the GCM predicts nearly identical moisture convergence change. In light of (2.9) or (3.1), this is surprising. Indeed, using the GCM results  $C' = -13 W m^{-2}$ ,  $R_t' = -7 W m^{-2}$ , and (2.9) for an inverse diagnosis, one gets an equivalent stability factor  $m = 0.54$ , significantly larger than 0.33 used in the theory. Interestingly, if (2.9) is applied to the GCM's DJF climatology ( $R_t = 48 W m^{-2}$ ,  $C = 134 W m^{-2}$ ), it gives  $m = 0.36$ , very close to the theory. This difference might be due to the nonlinearity in moist convection, or cloud-radiative interaction.

Given the simplicity of the analytical theory, one does not expect an accurate comparison with a particular GCM simulation. Rather, its strengths lie in its ability to explore the mechanisms and to analyze the processes and sensitivities. We now proceed to analyze some examples of this, namely, the processes controlling precipitation and ground temperature, the role of cloud radiative forcing, and effects of energy and water balance.

#### 4. Process analysis

##### a. Processes controlling precipitation change

For an albedo change, the analytical solution for precipitation in (3.8) reveals three controlling processes: the moisture convergence feedback (positive), the evaporation feedback (positive), and the cloud-radiative feedback (negative) (as depicted in Fig. 3). These feedback loops are initiated by the reduction in the top-of-the-atmosphere absorbed solar energy as increased surface albedo reflects more sunlight back into space. We term this ground albedo radiative forcing (GARF) similar to the definition of the cloud radiative forcing

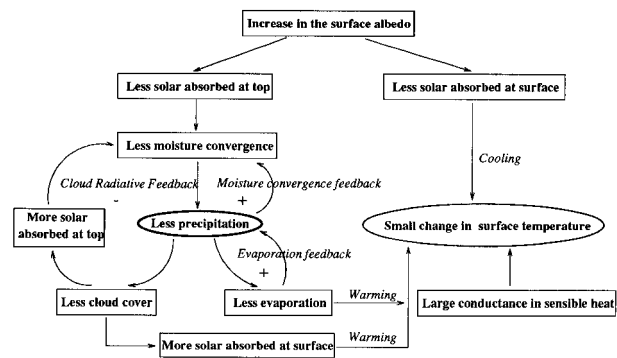


FIG. 3. Feedback loops in the energy and water budget in response to a surface albedo increase scenario. The left-hand side summarizes feedback loops affecting precipitation and column energy budget. The right-hand side summarizes feedback loops in the partitioning of the surface energy budget, which affects the ground temperature. Note that there are no feedbacks from the ground temperature to column energy budget due to the zero surface energy flux condition, indicated by the lack of arrows going from the rhs to the lhs of the diagram. The signs marked on the feedback loops associated with precipitation indicate positive or negative feedbacks. See text and Tables 3, 4 for quantitative assessment of the strengths of the feedback loops.

(CRF). This is not simply  $S_0 A'$ , but excludes the sunlight reflected and absorbed by cloud and atmosphere. This effect is absorbed in  $\theta_{TA}$  (appendix B). The three feedback terms appear in the denominator of (3.8). The moisture convergence feedback is associated with  $m$ , and is a positive feedback because  $m = (1 - \tilde{q})/\tilde{q}$  with  $\tilde{q}$  being the strength of moisture convergence effect. The evaporation feedback is associated with  $e$ , and is also a positive feedback, whereas the cloud radiative feedback increases the denominator, hence a negative feedback.

To quantify the relative importance of the three major feedback processes,  $P'$  dependence on the three parameters  $m$ ,  $e$ , and  $c$ , is plotted in Fig. 4. Table 3 compares the differences from the standard prediction (marked with  $\times$  in Fig. 4) to cases with each one of these three feedback processes absent in turn. By standard prediction, we mean the prediction using our best estimated value (Table 1;  $P'_{std} = 19.4 W m^{-2}$ ). For instance, setting  $e$  to zero rather than the standard value of 0.31 turns off the evaporation feedback while the other two are still on. The precipitation change predicted in this case will be called  $P'_{no\ feed}$ . The percentage difference is therefore defined as

$$\% \text{ difference} = \frac{P'_{std} - P'_{no\ feed}}{P'_{std}}$$

This is a measure of the effectiveness of the feedback process relative to a hypothetical case without this process.

Table 3 shows that without the moisture convergence, the precipitation would not change simply because there is no moisture supply to the atmosphere (but the wind convergence can change). The evaporation feedback has

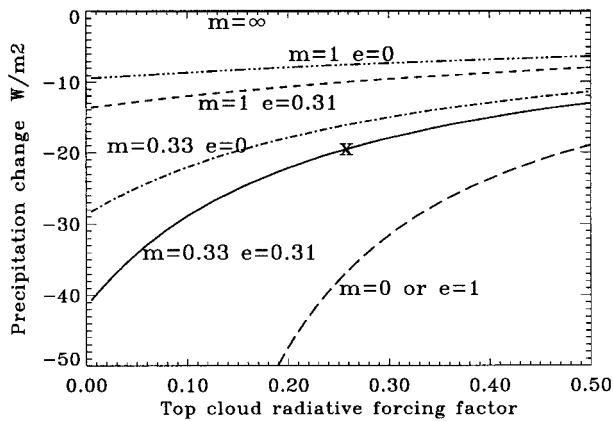


FIG. 4. Sensitivity of precipitation change  $P'$  to the strength of the top-cloud radiative forcing factor  $c_t$ , at various values of moisture convergence feedback factor  $m$  and evaporation feedback factor  $e$ ;  $\times$  marks the standard case with the best estimated parameter values in Tables 1 and 2; the extreme cases in Table 3 can be identified here.

a more moderate effect, increasing the precipitation by 18%. This difference in feedback strength is rooted in the standard parameter values  $m = 0.33$  and  $e = 0.31$ , which lump the final effects of moist convection and surface hydrology, respectively. The cloud effect comes in through the top-of-the-atmosphere cloud radiative forcing. When it is inactive, the precipitation change is 114% larger than the standard case; in other words, when it is active it reduces the rainfall change by about half. This provides an explanation for the seemingly large reduction in rainfall predicted by some earlier GCM studies with prescribed clouds (e.g., Nobre et al. 1991).

On the other extreme, if these feedbacks act too strongly, one can also estimate their influence on precipitation prediction. We define the percentage difference such that positive/negative feedbacks retain positive/negative sign:

$$\% \text{ difference} = \frac{P'_{\text{strong}} - P'_{\text{std}}}{P'_{\text{std}}},$$

where  $P'_{\text{strong}}$  is the precipitation change if a process is too strong. As one can see in Table 3, the precipitation response is 88% stronger for both full moisture convergence feedback and evaporation feedback, whereas a doubling in cloud feedback reduces  $P'$  by 35%. An interesting point is that when either moisture or evaporation feedback is at its full strength—that is,  $m(1 - e)$  becomes zero—the negative cloud feedback alone would be sufficient to limit precipitation.

Caution needs to be exercised in the quantitative interpretation of the above analysis because under these extreme situations, some of the linear assumptions made in the simple model may not hold well. It is nonetheless useful as a qualitative measure since some modeling studies may completely neglect an individual process such as cloud feedback.

TABLE 3. Sensitivity of precipitation change to the three feedback processes in extreme cases. The change in precipitation at best estimated parameter values (standard;  $m = 0.33$ ,  $e = 0.31$ ,  $c_t = 0.26$ ) is  $P'_{\text{std}} = -19.4 \text{ W m}^{-2}$ . The case “nofeed” is when a feedback is turned off while other two are set at their standard values. The case “strong” is when a feedback is stronger than standard. First numerical values in each column give  $P'$  in  $\text{W m}^{-2}$  in each case. The percentage differences are defined as:  $(P'_{\text{std}} - P'_{\text{nofeed}})/P'_{\text{std}}$  and  $(P'_{\text{strong}} - P'_{\text{std}})/P'_{\text{std}}$ .

	Moisture	Evaporation	Cloud
$P'_{\text{nofeed}}$	$\bar{q} = 0$ ( $m = \infty$ ) -0.0 +100%	$e = 0$ -16.0 +18%	$c_t = 0$ -41.6 -114%
$P'_{\text{strong}}$	$\bar{q} = 1$ ( $m = 0$ ) -36.5 +88%	$e = 1$ -36.5 +88%	$c_t$ doubled -12.7 -35%

A more precise measure of sensitivity to the feedback processes is to consider the difference in  $P'$  relative to a *small* change in the parameter values from the standard ones. A relative change in  $P'$  can be expressed as

$$\frac{dP'}{P'} = \frac{\partial P'}{\partial m} dm + \frac{\partial P'}{\partial e} de + \frac{\partial P'}{\partial c_t} dc_t.$$

Taking partial derivatives relative to  $m$ ,  $e$ , and  $c_t$  in (3.8), one obtains

$$-\frac{\partial P'}{\partial m} = \frac{(1 - e)}{m(1 - e) + c_t} = +1.41, \quad (4.1)$$

$$\frac{\partial P'}{\partial e} = \frac{m}{m(1 - e) + c_t} = +0.68, \quad (4.2)$$

$$\frac{\partial P'}{\partial c_t} = -\frac{1}{m(1 - e) + c_t} = -2.05. \quad (4.3)$$

A negative sign in the lhs of (4.1) is employed for clarity, since  $m$  decreases as the moisture convergence feedback becomes stronger. The numerical values are computed using the standard values in Table 1. A sensitivity of +0.68 to  $e$  means that, for instance, 10% more water recycled into atmosphere through evaporation [Eq. (2.10);  $\Delta e = 0.1$ ] would lead to a 6.8% increase in the magnitude of  $P'$ , and therefore a further decrease in  $P$ . One can see how the sensitivity to evaporation becomes higher as  $e$  itself increases because the denominator in (4.2) becomes smaller at larger  $e$ . For instance, at  $e = 0$ ,  $(\partial P')/(\partial e) = +0.56$ , and at  $e = 1$ ,  $(\partial P')/(\partial e) = +1.27$ . This effect is illustrated in Fig. 5. Similarly, the sensitivity to  $\bar{q}$  (or  $m$  with opposite sign) increases at larger  $\bar{q}$ , whereas the sensitivity to  $c_t$  becomes smaller at larger  $c_t$  (solid curve in Fig. 4). This tendency is not necessarily the result of being a positive or negative feedback because the second derivative of a function need not have the same sign as its first derivative, but it happens to hold for (3.8). Because of the nonlinearity in (3.8), while the percentages in Fig. 3 give an indication of the strength of each feedback process, the actual sensitivity depends on the basic state from which it is perturbed. Translating this into implications for GCM analysis, model-simulated anomalies can depend

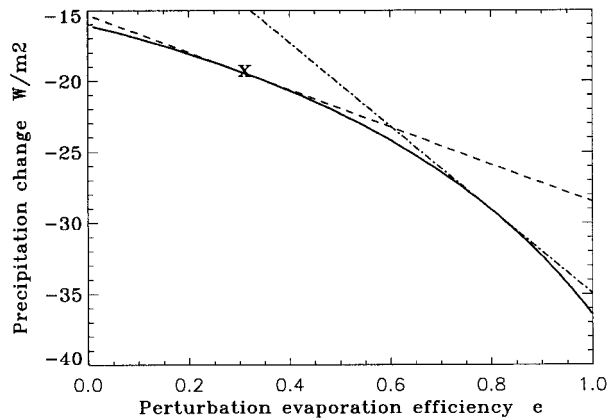


FIG. 5. Sensitivity of precipitation change  $P'$  to the strength of the perturbation evaporation efficiency  $e$  ( $m = 0.33$ ,  $c_t = 0.26$ ), showing the nonlinearity of the dependence. The sensitivity to the water recycling ability is higher at larger  $e$ , as shown by straight lines illustrating the different slopes at  $e = 0.31$  (dashed line) and  $e = 0.8$  (dash-dotted line).

on model climatology. This offers an explanation for why precipitation change in deforestation experiments can have even different signs in cases with different model-simulated climatologies (e.g., Polcher and Laval 1994; HD, their Table 1). In the current theory, this nonlinearity originates from the interaction of the processes, rather than the processes themselves, which are linearized here. Although we are not explicitly considering the seasonal cycle here, we also note that the seasonal variations in  $e$ ,  $m$ , and  $c_t$  would affect relative importance of these processes over the course of a seasonal cycle.

*b. Processes controlling ground temperature change*

Equation (3.11) gives an expression for the ground temperature  $T_s$  as a function of albedo change and various parameters. The processes controlling  $T'_s$  are illustrated in Fig. 3. Initially the reduction in GARF at the surface tends to cool the ground as more sunlight is reflected by a higher surface albedo ( $-15 \text{ W m}^{-2}$ ). However, as precipitation decreases, the evaporation decreases and takes less heat away from the ground ( $+6 \text{ W m}^{-2}$ ). At the same time reduced cloud cover allows more solar radiation to arrive at the ground than would otherwise ( $+6.5 \text{ W m}^{-2}$ ;  $-1 \text{ W m}^{-2}$  in longwave). These two negative feedbacks tend to cancel the initial shortwave reduction, resulting in a small residual ( $3.5 \text{ W m}^{-2}$ ) in the surface energy budget. This residual comes in the form of sensible heat and upward longwave radiation at surface, with the former dominating. In fact, since the surface roughness is high (recall that this is albedo change only), sensible heat flux is very efficient at transporting heat from the ground to the atmosphere. Whereas the right-hand side of (3.11) gives an already small residual energy, the longwave and sensible heat coefficients  $\epsilon_s$  and  $\zeta$  act as efficient conductors, further

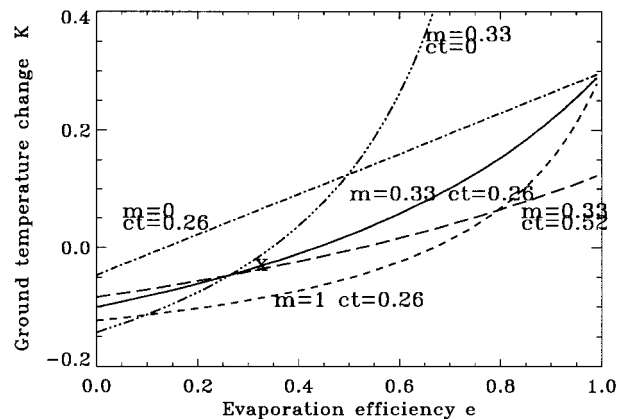


FIG. 6. Sensitivity of ground temperature change  $T'_s$  to the strength of the perturbation evaporation efficiency  $e$ , at various values of the moisture convergence feedback factor  $m$  and top-cloud radiative feedback factor  $c_t$ ; the surface CRF factor  $c_s$  is assumed to vary proportionally to  $c_t$ . Here  $\times$  marks the standard case with the best estimated parameter values in Tables 1 and 2; the extreme cases in Table 4 can be identified here.

reducing the heating or cooling effect, resulting in a small ground temperature change.

It is worth emphasizing that this set of feedbacks affecting ground temperature has no direct impact on the feedback loops affecting precipitation. This is seen diagrammatically in Fig. 3 by the lack of arrows from the rhs to the lhs of the figure. This is because of the surface energy balance condition (2.8). The ground temperature responds largely to satisfy the surface energy and water balances. The value of  $T_s$  is affected by the partitioning of surface energy, which has no direct effect on precipitation. The effect of energy versus water balance is further discussed in section 4d.

Sensitivity of ground temperature to moisture convergence, evaporation, and cloud effects are estimated in a way similar to that of precipitation. This is plotted in Fig. 6. The extreme cases where these processes are turned off or set too strong are listed in Table 4. Of particular interest is that an overestimation of the strength of either moisture convergence feedback and evaporation feedback can lead to a sign change in  $T'_s$  compared to the standard case. This is because the enhancement of the hydrological response increases the magnitude of reduction in evaporation and surface CRF, both having a negative feedback effect against the initial reduction of solar radiation at surface. This is seen in (3.11) as an increase in the second term in the curly brackets. In contrast not much sensitivity to cloud cover change alone is found, due to the partial cancellation of the CRF effect at the top and surface, seen in the  $c_t$  and  $c_s$  terms in (3.11). This is the case for change in the cloud cover-precipitation ratio  $\sigma_p$  so that  $c_t$  and  $c_s$  are proportional to each other. It would be more subtle if the relative contribution to top and surface radiation from clouds varies.

TABLE 4. Sensitivity of the ground temperature to the feedback processes in extreme cases; in kelvins;  $T'_{\text{std}} = -0.03$  K is the change in  $T_s$  at best estimated parameter values (standard; Table 1); “nofeed” is when that feedback is turned off while other two are set at their standard values, and “strong” is when the feedback is stronger than standard.

	Moisture	Evaporation	Cloud
$T'_{\text{nofeed}}$	$\tilde{q} = 0$ ( $m = \infty$ ) -0.14	$e = 0$ -0.1	$\sigma_p = 0$ -0.02
$T'_{\text{strong}}$	$\tilde{q} = 1$ ( $m = 0$ ) +0.06	$e = 1$ +0.3	$\sigma_p$ doubled -0.04

### c. Role of cloud radiative forcing

As discussed in previous subsections, CRF plays a very interesting role here. For precipitation, only the top-of-the-atmosphere CRF matters, a consequence of the surface total energy flux zero condition. The top-of-atmosphere radiation control on moisture convergence [Eq. (2.7)] puts the cloud radiative process in an important position. The role of cloud radiative forcing at the top and surface can be seen in the factors  $c_t$  and  $c_s$  as defined in section 3. In (3.9) and (3.10), the first term on the rhs is the shortwave contribution and the second term is the longwave contribution. Because cloud traps longwave radiation,  $\epsilon_{\sigma}$  is negative. In the shortwave band, the cloud reflects energy into space so that the shortwave and longwave CRFs have opposite signs and they tend to cancel each other. This cancellation also occurs at the surface. However, the net effect is such that the shortwave somewhat dominates (Table 1). The top-cloud radiative feedback factor  $c_t$  is about the same size as moisture and evaporation feedbacks combined  $m(1 - e)$  (Table 2), this negative feedback effectively reduces the sensitivity of precipitation response to further enhancement in the hydrological feedbacks.

The CRF at the surface is dominated by shortwave forcing ( $6.5 \text{ W m}^{-2}$  vs  $-1 \text{ W m}^{-2}$  for longwave) because the cloud-trapped longwave is mostly absorbed in the atmosphere by water vapor,  $\text{CO}_2$ , and other greenhouse gases, leaving little incident at the ground. The shortwave is also somewhat absorbed in the atmosphere, mostly by water vapor. This results in the net CRF factors at top and surface  $c_t$  and  $c_s$  being nearly the same. This gives rise to a subtlety in the ground temperature response (see section 4b): although the CRF at the surface has a warming effect on ground temperature (Fig. 3), the CRF at the top has an indirect cooling effect through its negative feedback on precipitation and therefore on evaporation the top CRF [Eq. (3.11)]. This leads to the relative insensitivity of ground temperature to cloud cover change.

ERBE finds a near cancellation of longwave CRF and shortwave CRF in the tropical climatology, with shortwave CRF somewhat larger (about  $70 \text{ W m}^{-2}$  and  $-100 \text{ W m}^{-2}$ , respectively, over the Amazon for January total cloud; Harrison et al. 1993). Our estimation gives per-

turbations of  $-4 \text{ W m}^{-2}$  and  $9 \text{ W m}^{-2}$  due to high and middle cloud (Table 2 and Fig. 2), with a noticeably larger shortwave effect compared to ERBE’s climatology. Interestingly, a CCM1-Oz/BATS deforestation run (Zhang et al. 1996) simulated a longwave and shortwave CRF ratio for control climate similar to ERBE but for change due to deforestation this ratio is similar to our estimation. Although this does not directly support our estimation because in their simulation factors other than albedo are also changed, this does indicate the perturbation slope may be different than the mean due to nonlinear effects. An analysis of ERBE radiative flux anomaly should be able to shed light on this.

### d. Effects of energy and water balance

A great simplification in this theory comes from the column energetic consideration in the moist static energy Eq. (2.7). As a consequence only the fluxes in and out of the whole atmosphere column are important. This, combined with the surface net energy flux zero condition (2.8) and the moist convective closure, leads to the interesting conclusion that moisture convergence depends on the top-of-atmosphere energy budget only [Eq. (2.9)].

There has been the concern that a possible warmer surface due to, say, reduced evaporation, can lead to more dry convection and therefore induces more convergence, a negative feedback mechanism (e.g., Eltahir and Bras 1993, though  $T_s$  barely warmed in the wet-season albedo change case we have analyzed here, see section 4b). The current theory puts these seemingly competing effects in a complete picture. In a moist convective region, land surface temperature is largely a response to the energy and water balance, rather than a forcing as in the case of sea surface temperature, due to land’s much lower heat capacity. It does not matter to moisture convergence how the surface energy is partitioned among sensible heat, evaporation, and radiation. The partitioning does make a difference in precipitation through the direct contribution from evaporation (2.5) but the magnitude of this contribution is more a result of surface water balance than energy balance, because the evaporation efficiency factor  $e$  is largely controlled by surface hydrology [see (2.10) and appendix A]. Frequent dry convection in the shallow boundary layer alone is not sufficient to drive rainfall-generating deep convection without enough energy and water supplies, such as what happens in an environment similar to the Sahara (Cook 1994).

It is of interest to note that the lack of energy closure exists in many tropical simple models for studying land-atmosphere-ocean interaction. For instance, in Zeng (1998) the evaporation feedback has an effect on moisture convergence by increasing convective latent heat release, making the precipitation sensitivity higher [his Fig. 1; also compare the denominators in his Eq. (7) and our Eq. (3.8)]. In fact, it is this understanding in

Zeng's analysis that has led to the present work. In the present framework evaporation contributes only to precipitation directly without interacting with the moisture convergence feedback loop. This is why Fig. 3 is plotted to show that the evaporation and moisture convergence feedbacks do not directly interact, whereas the cloud-radiative feedback interacts with both of them. This subtlety can also be seen in the arrangement of the three terms in the denominator of (3.8).

To a first-order approximation, the evaporation efficiency  $e$  is determined by the surface water budget (appendix A). It consists of direct contributions from evapotranspiration and interception loss, and is indirectly controlled by the runoff processes through their relation with precipitation and soil moisture. This links the surface water budget with the surface energy budget through evaporation [Eq. (2.8)], and therefore impacts ground temperature, as also noted by Shao and Henderson-Sellers (1996) in the Project for Intercomparison of Land Surface Parameterization Schemes. However, in the case studied here, there is no direct impact of surface water budget on atmospheric column energy budget due to the zero surface energy flux constraint.

The surface water budget is further linked to precipitation through the atmospheric water budget equation (2.5), because evaporation directly contributes to rainfall change. There has been much discussion on the role of water vapor recycling through evaporation (e.g., Eltahir and Bras 1996). To the extent current theory applies, this question can be largely side-stepped because of the constraint from the coupled energy and water budget consideration. Information about water recycling through evaporation alone is not sufficient in determining precipitation because in a thermally direct tropical atmospheric circulation system, energy input is necessary to induce large-scale circulation that sustains rainfall. If one wishes to consider the recycling issue in the current framework, an important factor that decides how much of the reevaporated water vapor is transported out of the region is the nondivergent wind component, which is determined at least as much by large-scale dynamics as by local thermodynamics. Whereas the theory predicts only the change in divergence, the nondivergent wind component can be diagnosed by introducing the momentum equations.

## 5. Concluding remarks

Motivated by the continuing concern and GCM studies on tropical deforestation, this work takes an analytical approach, following those of Charney (1975) and Eltahir and Bras (1993), and builds on the insight gained from many GCM analyses and our previous studies (Zeng et al. 1996; Zeng 1998). Our approach is to simplify the individual processes but focus on the interactions among them.

A consistent treatment of energy and water budget, in particular the column and surface energy budget,

proves critical. This is underlined because these energy constraints are not always enforced in tropical simple models (sections 2a, 4d), and deforestation GCM studies tend to focus on the surface energy budget only. In addition to using these energy and water constraints, the analytical framework is made possible by some key assumptions: 1) Moist convection imposes constraints on vertical temperature and humidity profiles and subsequent redistribution of energy occurs subject to this constraint (Arakawa and Schubert 1974; Betts and Miller 1986). 2) The feedback from the remote large-scale response occurs via convergence terms, whereas details of the spatial pattern of temperature and moisture response are negligible, so one does not need to solve the full dynamical equations. 3) Small perturbations on a climatologically deep convective region are considered so that the processes can be linearized. Simplification is achieved in the vertical by assumption 1, and in the horizontal by assumption 2. Mathematically, the theory becomes essentially a linear local analysis, whereas the vertical and horizontal structures can be diagnosed once the local perturbation is solved. Physically, the model includes nonlocal effects; for instance, moisture is supplied from adjacent regions.

The land surface-atmosphere physical interaction includes the exchanges of energy, water, and momentum, with the energy budget playing a central role. The net energy flux zero condition at the land surface resulting from the low ground heat capacity makes land-atmosphere exchange distinctly different from ocean-atmosphere exchange. As a result, land surface temperature is largely a response to the energy and water balance, rather than a forcing as in the case of sea surface temperature. Consequently, the moisture convergence does not depend on the detailed energy partitioning at the land surface. This energy constraint puts certain limits on the extent to which surface energy partitioning can influence the deforestation response. With energy consistency, the seemingly competing effects on precipitation due to less evaporation on one hand and subsequent surface warming on the other hand are also reconciled. The water budget is also important, both in the atmosphere and at the land surface. However, information about water recycling through evaporation alone is not sufficient to close the loop. It needs to be considered together with the energy budget because in the thermally direct tropical atmospheric circulation system, energy input is necessary to induce large-scale circulation that sustains rainfall (section 4d).

When the theory is applied to a wet-season albedo increase case, a precipitation decrease is found. This is initiated by the reduced ground albedo radiative forcing as increased surface albedo reflects more solar radiation into space. The positive moisture and evaporation feedbacks enhance this tendency substantially, with the moisture convergence feedback playing a prominent role. The moisture convergence feedback works by reducing the effective atmospheric stability, making the

heating more efficient at driving the moisture convergence. The evaporation directly contributes to precipitation through the atmospheric water budget equation (2.5) but does not directly interact with moisture convergence at this level of approximation. A significant negative feedback is due to the increased cloud radiative forcing as cloud cover decreases with less precipitation. This sheds light on why higher sensitivities are found in some GCM simulations with prescribed clouds. The shortwave and longwave cloud radiative forcings have opposite signs with shortwave effects dominating both at the top of the atmosphere and at the surface.

The sensitivity of precipitation perturbation to the strengths of individual processes are assessed. This sensitivity depends on the reference state parameter values. For instance, the sensitivity to evaporation feedback would be higher if the reference state value is higher. On the other hand the sensitivity to cloud radiative feedback becomes lower as the reference state cloud effect becomes stronger (section 4a). In GCM simulations, this nonlinearity implies a dependence of anomaly on model climatology.

The ground temperature is cooled initially by the reduced solar absorption at the ground. But negative feedbacks from reduced evaporation and increased downward solar radiation due to reduced cloud cover tend to cancel this cooling tendency, leaving a small residual in the surface energy budget. The highly effective sensible heat transport due to the rough surface further reduces the effect so the ground temperature is changed only by a small amount.

When predicted energy and water fluxes at the top of the atmosphere and the surface are compared to a recent RCCM2/BATS simulation for Amazon deforestation with evaporation matched to that of the GCM prediction, the agreement is generally good although with noticeable difference in the top-of-the-atmosphere solar radiation. Although the goal of the theory is not to seek a precise agreement with a particular GCM, this level of agreement is encouraging for such a simplified analytical model. The theory depicts the interaction among processes in a *closed* form, identifying the cause–response relationship. For instance, in the response to surface albedo increase, despite the importance of cloud feedbacks to shortwave at the surface, the precipitation response is largely independent of the surface temperature response. This is because the partitioning of the surface energy budget becomes less important to precipitation when the zero surface energy flux condition is included.

However, one must bear in mind the limitations of a simple model like this. Whereas we have made a great effort trying to nail down the parameter values associated with each process based on observation and physical considerations, they are open to questioning and refinement, as well as the way the processes are simplified. For instance, of particular concern is the role of diurnal cycle and mesoscale effects. Dirmeyer (1992)

found that decreased cloudiness at daytime and increased cloudiness at nighttime almost offset the effects of a small albedo change due to the daytime shortwave and nighttime longwave radiative effects. In a GCM simulation where the Amazon is deforested only to its 1988 level, Sud et al. (1996) found a significant evaporation decrease but a smaller reduction in precipitation due to an increase in moisture convergence. This is possibly associated with the subbasin-scale circulation induced by a warmer surface. Interestingly, in a similar simulation but only looking at a few individual rainfall events, Walker et al. (1995) found a decrease in moisture convergence as well as decreases in evaporation and precipitation. Cook (1994) found in an idealized GCM experiment that the surface moisture deficit can have different effects over the eastern and the western portions of a tropical continent, indicating that the coastal area and the interior Amazon may not respond in the same way. Zeng (1998) discussed the applicability of such a local analysis. Zeng et al. (1996) also point to the possibility of a change in SST in the surrounding ocean and subsequent feedbacks, especially to the coastal region, which is impacted by the diurnal sea breeze. Some of these complexities at finer spatial and temporal scales may be possible to parameterize in the future versions of a simple model. Another related issue is how these processes change over a seasonal cycle. In particular, during the dry season, the convection is not strong enough to establish an overall quasi-equilibrium between convection and large-scale dynamics. It is easier to handle if this amounts to only a seasonally varying relative moist stability factor  $m$ , but it can be more complicated if the decoupling of the planetary boundary layer and the free atmosphere has significant consequence. In the latter case some of the constraints due to moist convective closure need to be reassessed.

Despite the fact that it is still some distance away from fully answering the questions raised in the deforestation problem, the theoretical framework can be useful for the diagnosis and intercomparison of GCM simulations. As in the comparison with Hahmann and Dickinson (1997), the theory points to the potentially important areas to look at. For instance, most of the GCM analyses do not pay enough attention to the top-of-the-atmosphere radiation. Whereas much recent modeling effort focuses on the land surface hydrology, what differences the host GCMs make have been rarely studied. In this area, the present theory suggests that moist convection and cloud-radiative effects would be the key processes.

The wet-season albedo change case is excellent for the intercomparison of atmospheric component of the GCMs used in the deforestation study. Albedo change mainly perturbs the local thermodynamics, which is related to two of the most poorly understood and parameterized processes in current GCMs, namely the moist convective and cloud processes (e.g., Gates et al. 1995). The current theory suggests that despite the complex-

ities in deep convection, it also permits simplifications as well. A GCM simulation can be analyzed in terms of the theory, so the role of each individual process can be assessed. For instance, the relation (2.9) linking the water and energy budget can be tested. The diagnosed relative moist stability factor  $m$  can be compared with the direct estimate from model-simulated mean vertical temperature and humidity profiles. Then a comparison among GCMs would give a lumped signature of the moist convective parameterizations.

We underline that a consistent treatment of energy and water budget, both in the atmosphere and at the land surface, is critical in understanding land-atmosphere interaction. Constraints imposed by the energy and water balance requirement can already lead a long way in our understanding of the intertwining processes in the deforestation problem.

*Acknowledgments.* We are grateful to Andrea Hahmann for providing her thorough analysis of the RCCM2/BATS simulation, and to Chia Chou for providing his linearized longwave radiation package. This work started as we visited the Massachusetts Institute of Technology in 1995. We have benefited from discussions with R. Dickinson, P. Dirmeyer, E. Eltahir, K. Emanuel, K. Laval, J. Polcher, J. Shukla, J. Shuttleworth, Y. Sud, and X. Zeng. Comments from an anonymous reviewer and the editor G. Bonan have helped to improve the quality of the paper. This research was supported by NSF Grant ATM-9521389 and NOAA Grant NA46GP0244.

### APPENDIX A

#### An Analysis of Surface Water Budget

In this appendix we show the generality of the perturbation evaporation-precipitation relation (2.10) based on a single soil layer model that represents the root zone. The water budget equation in this layer is

$$\frac{\partial W}{\partial t} = P - E_I - R_s - E_T - R_g,$$

where  $W$  is the equivalent water depth per unit area and  $P$  is the precipitation. The total evaporation  $E$  can be expressed as the sum of the interception loss  $E_I$  and the evapotranspiration  $E_T$ . Here,  $R_s$  is the surface runoff (fast component) and  $R_g$  is the subsurface runoff (slow component). The order of the terms on the rhs is non-trivial because it represents the approximate timing of the occurrence of the processes.

For the water sinks, we parameterize them in general forms that functionally encompass what have been used in the current land surface schemes (e.g., Shao and Henderson-Sellers 1996). For interception loss,

$$E_I = E_I(P, R_n).$$

The intercepted water is not available for surface runoff:

$$R_s = \gamma_s(w)(P - E_I),$$

where  $w = W/W_0$  is the relative soil wetness and  $W_0$  is the field capacity and  $\gamma_s(w)$  is a nonlinear function of  $w$  to be specified. For instance,  $\gamma_s(w) = w^4$  returns the BATS formulation. This function lumps the effects of temporal and spatial variability of rainfall and surface characteristics, including potentially important factors like soil infiltration capacity (Lean et al. 1996). For evapotranspiration,

$$E_T = \beta(w)E_p(R_n),$$

where  $E_p$  is the potential evaporation and  $R_n$  is the net radiation absorbed at surface. It is noted that certain approximation has to be made in order to separate the  $w$  and  $R_n$  dependences if one starts with a formulation like the Penman-Monteith equation. But this separation is a matter of convenience rather than being essential for the purposes here. For subsurface runoff,

$$R_g = \gamma_g(w)R_{g0},$$

where  $R_{g0}$  is the subsurface runoff for a saturated soil layer.

In these parameterizations the dependent variables are  $w$ ,  $R_n$ , and  $P$ . The soil wetness dependent functions  $\beta(w)$ ,  $\gamma_s(w)$ ,  $\gamma_g(w)$  range from zero to one and can be highly nonlinear. These can be specified following the "semi-empirical" formulations of Koster and Milly (1997), or more physically based parameterizations such as Entekhabi and Eagleson (1989) if quantitative estimation is needed.

Before invoking the actual mathematical functions, the knowledge of the general functional dependence on  $w$ ,  $P$ , and  $R_n$  can already be very useful. The land surface water budget equation can be written in terms of these general functional dependences:

$$W_0 \frac{\partial w}{\partial t} = P - E_I(P, R_n) - R_s(w, P - E_I) - R_g(w) - E_T(w, R_n).$$

The perturbed water equation for a deforestation scenario is

$$\begin{aligned} W_0 \frac{\partial w'}{\partial t} + \left( \frac{\partial R_s}{\partial w} + \frac{\partial R_g}{\partial w} + \frac{\partial E_T}{\partial w} \right) w' \\ = \left( 1 - \frac{\partial E_I}{\partial P} \right) \left( 1 - \frac{\partial R_s}{\partial P} \right) P' \\ - \left\{ \frac{\partial E_I}{\partial R_n} \left( 1 - \frac{\partial R_s}{\partial P} \right) + \frac{\partial E_T}{\partial R_n} \right\} R'_n. \end{aligned} \quad (A.1)$$

This is a linear force-damped equation for  $w'$ . A complication is that  $P$ ,  $w$ ,  $R_n$ ,  $P'$ , and  $R'_n$  can have a seasonal cycle so they are functions of time. However, the damping term on the lhs is much larger than the time derivative term, which can be neglected to a good approximation. And our detailed analysis shows that for a typ-

ical tropical rain forest environment, the  $R'_n$  term is much smaller than the  $P'$  term on the rhs. This is due to the fact that in the Tropics the available energy is abundant and varies little throughout a year, so the evaporation is mainly controlled by water availability. Neglecting  $\partial w'/\partial t$  and  $R'_n$  terms, we can then solve (A1) for  $w'$ :

$$w' = \frac{\left(1 - \frac{\partial E_l}{\partial P}\right)\left(1 - \frac{\partial R_s}{\partial P}\right)}{\frac{\partial R_s}{\partial w} + \frac{\partial R_g}{\partial w} + \frac{\partial E_T}{\partial w}} P'. \quad (A.2)$$

Then the total evaporation change can be expressed as a linear function of  $P'$ :

$$E' = E'_l + E'_r = eP', \quad (A.2)$$

where the perturbation evaporation efficiency  $e$  is

$$e = \frac{\partial E_l}{\partial P} + \frac{\left(1 - \frac{\partial E_l}{\partial P}\right)\left(1 - \frac{\partial R_s}{\partial P}\right)}{1 + \left(\frac{\partial R_s}{\partial w} + \frac{\partial R_g}{\partial w}\right) / \frac{\partial E_T}{\partial w}}. \quad (A.3)$$

Note that in the second term on the rhs, the precipitation-dependent terms appear on the numerator, whereas the wetness-dependent terms appear on the denominator. Using the detailed parameterizations and taking derivatives,  $e$  can be written as

$$e = \frac{\partial E_l}{\partial P} + \frac{\left(1 - \frac{\partial E_l}{\partial P}\right)(1 - \gamma_s)}{1 + \left\{ (P - E_l) \frac{\partial \gamma_s}{\partial w} + R_{g0} \frac{\partial \gamma_g}{\partial w} \right\} / \left( E_p \frac{\partial \beta}{\partial w} \right)}. \quad (A.4)$$

The rhs contains the quantities at reference state from which the perturbation is made. A large amount of information exists in (A4). The factor  $e$  consists of contributions from interception loss (first term on the rhs) and evapotranspiration (second term on the rhs), which is indirectly controlled by the runoff processes through their dependence on precipitation and soil moisture. Because of the nonlinearities, this ratio between evaporation and precipitation perturbations can be different from that between the totals. A seasonal variation in  $e$  is also apparent as the control climate has a seasonal cycle. Interestingly, the seasonal variation in reference state  $R_n$ , therefore in  $E_l$  and  $E_p$ , is allowed in (A4), only that its perturbation has been neglected.

## APPENDIX B

### The Parameterization of Shortwave Radiation and Cloud Albedo

We assume a single cloud-atmosphere layer with reflectivity  $\alpha$  and absorptivity  $a$ , and a surface with albedo

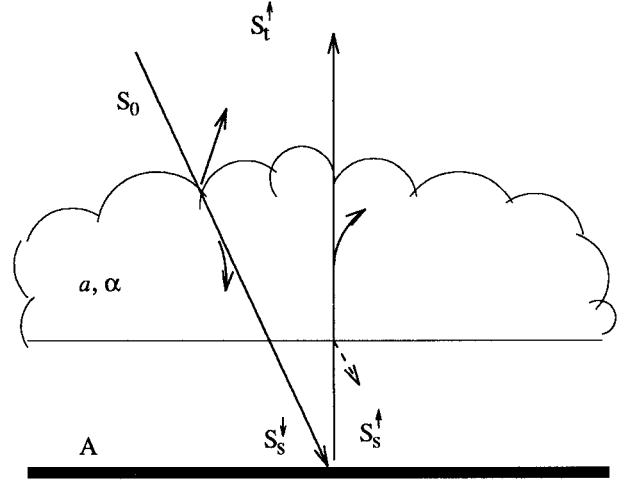


FIG. B1. A simple shortwave parameterization scheme, assuming a single cloud-atmosphere layer with reflectivity  $\alpha$  and absorptivity  $a$ , and a surface with albedo  $A$ ; multiple reflection is truncated at cloud base (broken arrow).

$A$  (Fig. B1). A two-stream approximation is used, with incoming solar radiation at the top reflected and absorbed before it reaches the surface. Then the solar radiation reflected by the surface also goes through reflection and absorption before it exits the atmosphere into space. This can be solved by either a closed form solution or multiple reflection technique (Kiehl 1992). For our application, we assume a single reflection at surface. This is equivalent to neglecting a higher-order term  $A\alpha$  against  $A$  or  $\alpha$  (cf. Kiehl's solution and ours) because both are much smaller than unity. Detailed calculation shows this results in less than 10% error. The main advantage of making this approximation is not numerical, but rather the conceptual simplification.

By tracing the light ray and truncating at the first reflection at cloud base, one easily obtains the fluxes at the top and surface:

$$\begin{aligned} S_s^\downarrow &= (1 - \alpha)(1 - a)S_0, \\ S_s^\uparrow &= (1 - \alpha)(1 - a)AS_0, \\ S_t^\uparrow &= \{(1 - \alpha)^2(1 - a)^2A + \alpha\}S_0, \end{aligned}$$

where  $S_0$  is the incoming solar radiation at the top of the atmosphere. By definition, the planetary albedo is

$$A_p = (1 - \alpha)^2(1 - a)^2A + \alpha. \quad (B.1)$$

Given a small perturbation in cloud and surface albedo  $\alpha'$  and  $A'$ , one can linearize the above expressions to obtain the perturbed fluxes:

$$\begin{aligned} S_s^{\downarrow\prime}/S_0 &= -\theta_{s\alpha}\alpha', \\ S_s^{\uparrow\prime}/S_0 &= \theta_{sA}A', \\ S_t^{\uparrow\prime}/S_0 &= \theta_{tA}A' + \theta_{t\alpha}\alpha'. \end{aligned} \quad (B.2)$$

The net downward fluxes are

$$S'_i/S_0 = -\theta_{iA}A' - \theta_{i\alpha}\alpha', \quad (\text{B.3})$$

$$S'_s/S_0 = -\theta_{sA}A' - \theta_{s\alpha}\alpha'. \quad (\text{B.4})$$

In principle, one can linearize more complicated parameterizations in a similar form. In our simple parameterization, the linearized coefficients are  $\theta_{i\alpha} = 1$ ,  $\theta_{s\alpha} = (1 - a)$ ,  $\theta_{sA} = (1 - \alpha)(1 - a)$ ,  $\theta_{iA} = (1 - \alpha)^2(1 - a)^2$ , where the parameters on the rhs take their reference state values.

For quantitative estimation of the reference state values  $\alpha$  and  $a$ , we use the ERBE observed planetary albedo over the wet-season Amazon [Harrison et al. (1993), their Fig. 2a,  $A_p \approx 0.35$ ] and their estimated global mean absorption (Harrison et al. Fig. 1,  $Q_s/S_0 \approx 0.19$ ), which is mainly due to water vapor. The surface albedo is taken to be 0.13. Equations (B1) and (B2) are then inverted to give an estimation for  $\alpha$  and  $a$ . A solar zenith angle correction is made in the reflected flux at surface in the estimation.

The cloud albedo depends on cloud type and characteristics, cloud cover, and solar zenith angle. The assumption is made that cloud characteristics does not vary much in a specified climatic region, so cloud albedo is roughly proportional to cloud cover for a particular cloud type:

$$\alpha = \alpha_\sigma \sigma,$$

where  $\sigma$  is cloud cover (cloud amount). An important issue is the solar zenith angle dependence of cloud albedo that has a diurnal and seasonal variation, making the cloud-radiation interaction nonlinear. In deriving a "mean"  $\alpha_\sigma$ , we assume a typical solar zenith angle for the Tropics, and use Chou's (1997) linear fit of coefficients to the Bishop and Rossow (1991) parameterization, where cloud type and solar zenith angle-dependent reflectivity were calculated based on the Mie scattering theory. The parameter values are listed in Table 1.

#### REFERENCES

- Arakawa, A., and W. H. Schubert, 1974: Interaction of a cumulus cloud ensemble with the large-scale environment. Part I. *J. Atmos. Sci.*, **31**, 674–701.
- Betts, A. K., and M. J. Miller, 1986: A new convective adjustment scheme. Part II: Single column tests using GATE wave, BOMEX, ATEX and arctic air-mass data sets. *Quart. J. Roy. Meteor. Soc.*, **112**, 693–709.
- Bishop, J. K. B., and W. B. Rossow, 1991: Spatial and temporal variability of global surface solar irradiance. *J. Geophys. Res.*, **96**, 16 839–16 858.
- Charney, J. G., 1975: Dynamics of deserts and droughts in Sahel. *Quart. J. Roy. Meteor. Soc.*, **101**, 193–202.
- Chou, C., 1997: Simplified radiation and convection treatments for large-scale tropical atmospheric modeling. Ph.D. thesis, University of California, Los Angeles, 215 pp.
- , and J. D. Neelin, 1996: Linearization of a longwave radiation scheme for intermediate tropical atmospheric models. *J. Geophys. Res.*, **101**, 15 129–15 145.
- Cook, K. H., 1994: Mechanisms by which surface drying perturbs tropical precipitation fields. *J. Climate*, **7**, 400–413.
- Dickinson, R. E., and P. J. Kennedy, 1992: Impacts on regional climate of Amazon deforestation. *Geophys. Res. Lett.*, **19**, 1947–1950.
- , A. Henderson-Sellers, and P. J. Kennedy, 1993: Biosphere–Atmosphere Transfer Scheme (BATS) version 1e as coupled to the NCAR Community Climate Model. NCAR Tech. Note NCAR/TN-387+STR, 72 pp.
- Dirmeyer, P. A., 1992: GCM studies of the influence of vegetation on the general circulation: The role of albedo in modulating climate change. Ph.D. thesis, University of Maryland, 227 pp.
- Eltahir, E. A. B., and R. L. Bras, 1993: On the response of the tropical atmosphere to large-scale deforestation. *Quart. J. Roy. Meteor. Soc.*, **119**, 779–793.
- , and —, 1994: Sensitivity of regional climate to deforestation in the Amazon Basin. *Adv. Water Resour.*, **17**, 101–115.
- , and —, 1996: Precipitation recycling. *Rev. Geophys.*, **34**, 367–378.
- Emanuel, K. A., J. D. Neelin, and C. S. Bretherton, 1994: On large-scale circulations in convecting atmospheres. *Quart. J. Roy. Meteor. Soc.*, **120**, 1111–1143.
- Entekhabi, D., and P. S. Eagleson, 1989: Land surface hydrology parameterization for atmospheric general circulation models including subgrid scale spatial variability. *J. Climate*, **2**, 816–831.
- Gates, W. L., and Coauthors, 1996: Climate models—Evaluation. *Climate Change 1995: The Science of Climate Change*, J. T. Houghton, L. G. M. Filho, B. A. Callander, N. Harris, A. Kattenberg, and K. Maskell, Eds., Cambridge University Press, 229–284.
- Hahmann, A. N., and R. E. Dickinson, 1997: RCGM2/BATS model over tropical South America: Applications to tropical deforestation. *J. Climate*, **10**, 1944–1964.
- Harrison, E. F., P. Minnis, B. R. Barkstrom, and G. G. Gibson, 1993: Radiation budget at the top of the atmosphere. *Atlas of Satellite Observations Related to Global Change*, R. J. Gurney, J. L. Foster, and C. L. Parkinson, Eds., Cambridge University Press, 19–38.
- Held, I. M., and A. Y. Hou, 1980: Nonlinear axially symmetric circulations in a nearly inviscid atmosphere. *J. Atmos. Sci.*, **37**, 515–533.
- Kiehl, J. T., 1992: Atmospheric general circulation modeling. *Climate System Modeling*, K. E. Trenberth, Ed., Cambridge University Press, 319–370.
- Koster, R. D., and P. C. D. Milly, 1997: The interplay between transpiration and runoff formulations in land surface schemes used with atmospheric models. *J. Climate*, **10**, 1578–1591.
- Lean, J., C. B. Bunton, C. A. Nobre, and P. R. Rowntree, 1996: The simulated impact of Amazonian deforestation on climate using measured ABRACOS vegetation characteristics. *Amazon Deforestation and Climate*, J. H. C. Gash, C. A. Nobre, J. M. Roberts, and R. L. Victoria, Eds., John Wiley, 549–576.
- Manzi, A. O., and S. Planton, 1996: A simulation of Amazonian deforestation using a GCM calibrated with ABRACOS and ARME data. *Amazon Deforestation and Climate*, J. H. C. Gash, C. A. Nobre, J. M. Roberts, and R. L. Victoria, Eds., John Wiley, 505–529.
- Neelin, J. D., and J.-Y. Yu, 1994: Modes of tropical variability under convective adjustment and the Madden-Julian oscillation. Part I: Analytical results. *J. Atmos. Sci.*, **51**, 1876–1894.
- Nobre, C., P. J. Sellers, and J. Shukla, 1991: Amazonian deforestation and regional climate change. *J. Climate*, **4**, 957–988.
- Oberhuber, J. M., 1988: An atlas based on the COADS data set: The budgets of heat buoyancy and turbulent kinetic energy at the surface of the global ocean. Max-Planck Institut für Meteorologie Rep. 15. [Available from Max-Planck Institut für Meteorologie, Bundesstrasse 55, D-2000, Hamburg 13, Germany.]
- Polcher, J., 1995: Sensitivity of tropical convection to land surface processes. *J. Atmos. Sci.*, **52**, 3143–3161.
- , and K. Laval, 1994: A statistical study of regional impact of deforestation on climate in the LMD GCM. *Climate Dyn.*, **19**, 205–219.

- Rossow, W. B., and R. A. Schiffer, 1991: ISCCP cloud data products. *Bull. Amer. Meteor. Soc.*, **72**, 2–20.
- Shao, Y., and A. Henderson-Sellers, 1996: Modeling soil moisture: A project for intercomparison of land surface parameterization schemes phase 2(b). *J. Geophys. Res.*, **101**, 7227–7250.
- Shuttleworth, W. J., 1988: Evaporation from Amazonian rain forest. *Proc. Roy. Soc. London B*, **233**, 321–346.
- Slingo, A., and J. M. Slingo, 1991: Response of the National Center for Atmospheric Research community climate model to improvements in the representation of clouds. *J. Geophys. Res.*, **96**, 15 341–15 357.
- Sud, Y. C., R. Yang, and G. K. Walker, 1996: Impact of in situ deforestation in Amazonia on the regional climate—General circulation model simulation study. *J. Geophys. Res.*, **101**, 7095–7109.
- Walker, G. K., Y. C. Sud, and R. Atlas, 1995: Impact of ongoing Amazonian deforestation on local precipitation: A GCM simulation study. *Bull. Amer. Meteor. Soc.*, **76**, 346–361.
- Webster, P. J., 1981: Mechanisms determining the atmospheric response to sea surface temperature anomalies. *J. Atmos. Sci.*, **38**, 554–571.
- Williamson, D. L., J. T. Kiehl, V. Ramanathan, R. E. Dickinson, and J. J. Hack, 1987: Descriptions of NCAR Community Climate Model (CCM1). NCAR Tech. Note TN-285+STR, 112 pp.
- Yu, J.-Y., C. Chou, and J. D. Neelin, 1998: Estimating the gross moist stability of the tropical atmosphere. *J. Atmos. Sci.*, **55**, 1354–1372.
- Zebiak, S. E., 1986: Atmospheric convergence feedback in a simple model for El Niño. *Mon. Wea. Rev.*, **114**, 1263–1271.
- Zeng, N., 1998: Understanding climate sensitivity to tropical deforestation in a mechanistic model. *J. Climate*, **11**, 1969–1975.
- , R. E. Dickinson, and X. Zeng, 1996: Climatic impact of Amazon deforestation—A mechanistic model study. *J. Climate*, **9**, 859–883.
- Zhang, H., A. Henderson-Sellers, and K. McGuffie, 1996: Impacts of tropical deforestation. Part I: Process analysis of local climatic change. *J. Climate*, **9**, 1497–1517.